Method for deriving Hopf and saddlenode bifurcation hypersurfaces and application to a model of the Belousov–Zhabotinskii system

Bruce L. Clarke and Weimin Jiang

Citation: The Journal of Chemical Physics **99**, 4464 (1993); doi: 10.1063/1.466073
View online: http://dx.doi.org/10.1063/1.466073
View Table of Contents: http://scitation.aip.org/content/aip/journal/jcp/99/6?ver=pdfcov
Published by the AIP Publishing

Method for deriving Hopf and saddle-node bifurcation hypersurfaces and application to a model of the Belousov–Zhabotinskii system

Bruce L. Clarke and Weimin Jiang
Department of Chemistry, University of Alberta, Edmonton, Alberta T6G 2G2, Canada

(Received 25 August 1992; accepted 2 June 1993)

Chemical mechanisms with oscillations or bistability undergo Hopf or saddle-node bifurcations on parameter space hypersurfaces, which intersect in codimension-2 Takens–Bogdanov bifurcation hypersurfaces. This paper develops a general method for deriving equations for these hypersurfaces in terms of rate constants and other experimentally controllable parameters. These equations may be used to obtain better rate constant values and confirm mechanisms from experimental data. The method is an extension of stoichiometric network analysis, which can obtain bifurcation hypersurface equations in special (**h**,**j**) parameters for small networks. This paper simplifies the approach using Orlando's theorem and takes into consideration Wegscheider's thermodynamic constraints on the rate constants. Large realistic mechanisms can be handled by a systematic method for approximating networks near bifurcation points using essential extreme currents. The algebraic problem of converting the bifurcation equations to rate constants is much more tractable for the simplified networks, and agreement is obtained with numerical calculations. The method is illustrated using a seven-species model of the Belousov–Zhabotinskii system, for which the emergence of Takens–Bogdanov bifurcation points is explained by the presence of certain positive and negative feedback cycles.

I. INTRODUCTION

Every chemical mechanism has a "dynamical phase diagram" which divides parameter space into regions with various kinds of qualitative dynamics. When a mechanism can have both oscillations and bistability, the separating curve on the phase diagram usually terminates in Takens–Bogdanov bifurcation points (TB points) or double zero points. A TB point is analogous to the triple point of a liquid–gas–solid phase diagram.

Boissonade and De Kepper[1] studied a very simple two-species mechanism with oscillations and bistability. They discovered the presence of many small regions with different types of qualitative dyanamics close to the TB point. A detailed analysis of the possibilities by Guggenheimer[2] has been followed by more recent mathematical studies.[3,4]

This paper shows how to derive approximate equations for the Hopf and saddle-node bifurcation surfaces of chemical reaction networks. The most difficult challenge is to obtain equations which are valid near the TB points. The phase diagram in these regions is very sensitive to the chemical mechanism because feedback cycles determine the delicate balance between stability and instability. Any change in the mechanism that affects important feedback cycles can drastically change the phase diagram.

Attempts to confirm mechanisms by comparing theoretical and experimental phase diagrams have so far relied on numerical phase diagram calculations. Olsen and Epstein[5] examined the Citri–Epstein mechanism of the chlorite–iodide reaction and found good agreement with experiment. Ringland[6] made extensive calculations on a seven-species extended oregonator[7] model, known as the Showalter–Noyes–Bar-Eli[8] (SNB) model. He showed that the experiments could not be matched by adjusting rate constants. In this paper we will use the SNB model as an example to illustrate a general method of deriving equations for bifurcation hypersurfaces. The reasons why Ringland was unable to make the mechanism match experiment will become clear.

The first step in obtaining equations for the Hopf and saddle-node bifurcation curves uses an approach called stoichiometric network analysis[9–13] (SNA). This approach yields equations in special (**h**,**j**) parameters that cannot be compared directly with numerical calculations, which use rate constants. To apply the method to realistic networks we make several improvements in the approach. First, large complex realistic networks are approximated by excluding all but the essential reactions. This paper develops a method for determining essential reactions by ranking the extreme currents. Second, we show how the equations obtained by SNA for the approximate network may be expressed in terms of rate constants. The resulting approximate bifurcation equations are then compared with the exact numerically computed curves. We study how the qualitative agreement between the curves is affected by various approximations. We show how the dependence of the bifurcation curves on the important rate constants may be used to shift the curves to agree with experiment. From the fact that opposite shifts are required to make saddle-node and Hopf curves match experiments, we agree with Ringland that matching is not possible.

This paper uses Orlando's theorem for the first time in the context of SNA. The theorem greatly simplifies the criteria used for Hopf bifurcation curves. In addition, it shows that when a Hopf bifurcation curve's equation is followed on the other side of a TB point, the curve represents points where the eigenvalues are symmetrically positioned on opposite sides of the imaginary axis. This "symmetric eigenvalue curve" (SE curve) eventually passes through another TB point and emerges as the original

 0021-9606/93/99(6)/4464/15/$6.00

Hopf bifurction curve to form a closed loop. Only certain global arrangements of the bifurcation regions have the required loops.

Wegscheider recognized that rate constants must satisfy mathematical conditions to agree with thermodynamics. Such a condition occurs in the SNB model. We derive a new version of Wegscheider's condition in terms of the (**h**,**j**) parameters. The SNB rate constants used by Ringland must be changed to meet the Wegscheider condition but the bifurcation curves are not affected.

As a practical application of this approach, we show that adding reactions to the SNB model which are believed to occur in the real system should improve the agreement with experiment.

Another SNA-based approach for obtaining rate constants has been developed by Hynne, Sørensøn and Møller.[14,15] For the extended oregonator model, they obtained rate constants that match data from oscillation quenching experiments near supercritical Hopf bifurcation hypersurfaces using optimization over the current polytope. Their approach is complementary to ours. Our equations can be matched to the location of saddle-node and subcritical Hopf bifurcations while HSM's approach does not use such information.

II. EQUATIONS FOR THE BIFURCATION HYPERSURFACES ON THE PHASE DIAGRAM

An updated version of basic ideas of SNA was presented in Secs. III and IV of the paper on the oxalate–persulfate–silver system.[16] This section introduces two refinements—the Routh array and Orlando's theorem. The latter reduces the many Hopf bifurcation hypersurface equations $\Delta_i=0$, $i=1,...,d-1$ used in earlier treatments to the single equation $\Delta_{d-1}=0$. The Routh array approach makes it easier to understand why one of the conditions $\alpha_i=0$, $i=1,...,d-1$ is often a good approximation for $\Delta_{d-1}=0$.

In a chemical network with n intermediate species and r reactions, the dynamics of concentration perturbations $\Delta\mathbf{X}=\mathbf{X}-\mathbf{X}_0$ near a steady state $\mathbf{X}_0$ is given by the linearized equation

$$\frac{d\Delta\mathbf{X}}{dt}=\mathsf{M}(\mathbf{p})\Delta\mathbf{X}. \tag{1}$$

The Jacobian matrix $\mathsf{M}(\mathbf{p})$ is a function of a parameter vector $\mathbf{p}$ and has the form

$$\mathsf{M}(\mathbf{p})=\mathsf{N}\,\mathrm{diag}(\mathbf{v})\mathsf{K}^t\,\mathrm{diag}(\mathbf{X}_0^{-1}). \tag{2}$$

N is the n by r stoichiometric matrix, $\mathbf{v}$ is the reaction rate vector at the steady state $\mathbf{X}_0$, and K is the n by r kinetic matrix. K gives the order of each species in each reaction. The parameter vector $\mathbf{p}$ can be the (**k**,**C**) parameters (rate constants), or the (**h**,**j**) parameters. In terms of (**h**,**j**) parameters,

$$\mathsf{M}(\mathbf{h},\mathbf{j})=\mathsf{N}\,\mathrm{diag}(\mathsf{E}\mathbf{j})\mathsf{K}^t\,\mathrm{diag}(\mathbf{h}), \tag{3}$$

where we have made use of

$$\mathbf{v}=\mathsf{E}\mathbf{j}, \tag{4}$$

$$\mathbf{h}=\mathbf{X}_0^{-1}, \tag{5}$$

and E is the matrix of extreme currents. The (**h**,**j**) parameters will be explained later for the SNB model example.

Steady state stability is determined by the eigenvalues of $\mathsf{M}(\mathbf{p})$, which are the roots λ of the characteristic equation

$$|\lambda\mathbf{I}-\mathsf{M}(\mathbf{p})|=\lambda^n+\alpha_1(\mathbf{p})\lambda^{n-1}+\alpha_2(\mathbf{p})\lambda^{n-2}+\cdots+\alpha_n(\mathbf{p})=0. \tag{6}$$

When all eigenvalues lie in the left-half complex plane, the steady state is stable. When one or more eigenvalues lie in the right-half complex plane, the steady state is unstable. The transition case occurs on hypersurfaces in the high-dimensional space of the parameter vector $\mathbf{p}$. These divide the parameter space into the regions of the dynamical phase diagram according to the bifurcation that occurs at each hypersurface.

Let the general network have d independent intermediates ($d\leqslant n$). The dynamical system has dimension d. When $d<n$ there are $n-d$ independent constants of the motion and

$$\alpha_{d+1}(\mathbf{p})\equiv\alpha_{d+2}(\mathbf{p})\equiv\cdots\equiv\alpha_n(\mathbf{p})\equiv 0.$$

The factor λ^{n-d} in Eq. (6) yields $n-d$ constant eigenvalues $\lambda=0$, which will not be discussed further. The coefficients $\alpha_1(\mathbf{p}),...,\alpha_d(\mathbf{p})$ determine how the other eigenvalues depend on $\mathbf{p}$.

The number of eigenvalues in the right-hand half of the complex plane equals the number of sign changes in the first row of the *Routh array*[17]

$$\mathsf{R}=\left(1\quad\Delta_1\quad\frac{\Delta_2}{\Delta_1}\quad\frac{\Delta_3}{\Delta_2}\quad\frac{\Delta_4}{\Delta_3}\quad\cdots\quad\frac{\Delta_d}{\Delta_{d-1}}\right), \tag{7}$$

where Δ_i, $i=1,...,d$, is the $i\times i$ principal minor of the array

$$\begin{pmatrix}\alpha_1(\mathbf{p}) & \alpha_3(\mathbf{p}) & \alpha_5(\mathbf{p}) & \alpha_7(\mathbf{p}) & \cdots\\ 1 & \alpha_2(\mathbf{p}) & \alpha_4(\mathbf{p}) & \alpha_6(\mathbf{p}) & \cdots\\ 0 & \alpha_1(\mathbf{p}) & \alpha_3(\mathbf{p}) & \alpha_5(\mathbf{p}) & \cdots\\ 0 & 1 & \alpha_2(\mathbf{p}) & \alpha_4(\mathbf{p}) & \cdots\\ \cdots & \cdots & \cdots & \cdots & \cdots\end{pmatrix}, \tag{8}$$

and is called the ith *Hurwitz determinant*. For stable steady states not on transition hypersurfaces, R has the sign pattern $(+,+,+,...,+)$, which has no sign changes and hence no eigenvalues are in the right-half complex plane.

The elements in right-hand column of Δ_d are zero except α_d because $\alpha_i=0$ when $i>d$. Expanding Δ_d yields

$$\Delta_d=\alpha_d\Delta_{d-1}.$$

Hence the last element of R is α_d. If the steady state is stable and a parameter change makes α_d negative, the sign pattern becomes $(+,+,...,+,-)$. One sign change indicates one eigenvalue has crossed into the right-hand complex plane. Such a transition to instability occurs with

$$\alpha_d(\mathbf{p})=0. \tag{9}$$

and is a *saddle-node bifurcation*. This is a fold in the steady state manifold where the two steady states near the fold are stable and unstable.

At Hopf bifurcations $\alpha_d > 0$ so the last sign is "+". If all Hurwitz determinants are positive except Δ_i, for some $i<d$, the only negative ratios in R are Δ_i/Δ_{i-1} and Δ_{i+1}/Δ_i and the sign pattern is $(+,+,...,+,-,-,+,...,+)$. This pattern with two sign changes indicates two complex conjugate eigenvalues have crossed the imaginary axis, which occurs at a *Hopf bifurcation*. Hopf bifurcations occur whenever **p** crosses transversally through the hypersurface $\Delta_i(\mathbf{p})=0$ with all other Hurwitz determinants positive.

Previous papers on SNA used all Hurwitz determinants; however, we now use Orlando's theorem[18] to prove that only Δ_{d-1} is needed. The theorem says

$$\Delta_{d-1}=\prod_{j<k}^{1,...,d}(-\lambda_j-\lambda_k), \tag{10}$$

with the product over all pairs of eigenvalues. At a Hopf bifurcation point **p**, the factor $(-\lambda_j-\lambda_k)$ for the pair that crosses the imaginary axis is zero. Hence, $\Delta_{d-1}(\mathbf{p})$ changes sign at the Hopf bifurcation. It is therefore unnecessary to consider $\Delta_i(\mathbf{p})$ for $i=1,...,d-2$. Thus every Hopf bifurcation point satisfies

$$\Delta_{d-1}(\mathbf{p})=0. \tag{11}$$

At first it appears unlikely that two Hurwitz determinants would change sign at a bifurcation point. If so, the sign pattern just inside the unstable region is $(+,+,...,+,-,+)$. Sign changes in the other interior elements of R would only occur further inside.

Later we will see this assumption is wrong. Several Hurwitz determinants often change sign at almost the same **p**. For many networks the most important terms in Eq. (8) come from the product of diagonal elements,

$$\Delta_i=\alpha_1\alpha_2\cdots\alpha_i+\text{negligible terms}. \tag{12}$$

The dominant terms in R are then

$$\mathrm{R}=(1,\alpha_1,\alpha_2,...,\alpha_d). \tag{13}$$

Suppose feedback cycles involving a certain set of k intermediates produce negative terms in α_k. Because closely related terms appear in the expansions of α_i for $i=k,...,d$, a small change in **p** that makes α_k change sign may also make other α_i's change sign. Hence, many of the last $d-k+1$ elements of R may change sign almost simultaneously. The calculated sign pattern a "small step" into an unstable Hopf bifurcation region is often not the expected pattern $(+,+,...,+,-,+)$, which means other Δ_i's have changed sign very close to $\Delta_{d-1}=0$.

Hopf bifurcation hypersurfaces can be studied numerically by following Eq. (11) using continuation methods. Numerical difficulties arise if the algorithm jumps to other solutions which are present because Orlando's theorem says $\Delta_{d-1}=0$ when any two eigenvalues add to zero. Different pairs of eigenvalues produce solutions like the layers of an onion, and Hopf bifurcations occur only on the outer layer.

III. GLOBAL STRUCTURE OF SADDLE-NODE AND HOPF BIFURCATION HYPERSURFACES

When chemical reaction networks are parametrized using the (**h**,**j**) parameters, the dynamical phase diagram has global mathematical properties that are not always present in the general dynamical system. This section examines the possible phase diagrams of stoichiometric networks.

Dynamical phase diagram hypersurfaces are characterized by mathematicians as "codimension one bifurcation points of first order structurally unstable vector fields." Hale and Koçak[19] state the six possibilities in Theorem 13.24 and illustrate them in Fig. 13.6. The two types of local bifurcations are the Hopf and saddle node. The four types of global bifurcations are the saddle-node bifurcation on a loop (SNL), the saddle-node bifurcation of a periodic orbit (SNP), the homoclinic loop bifurcation (HL), and the breaking of a saddle connection (SC).

The saddle node bifurcations represent a folding of the steady state manifold. We follow the notation of other authors[5,6] and restrict the term saddle node (SN) to folds with a stable steady state near the bifurcation point. If both steady states are unstable the term *saddle-node plus* (SN^+) will be used.

The Hopf and SN bifurcation points are subsets of the solutions of Eq. (11) and Eq. (9). When **p** is an arbitrary parameter system, there may be $0,1,2\cdots$ steady states for a given **p**. Each steady state has different functions α_d (**p**) and Δ_{d-1} (**p**). This complicates the analysis for arbitrary parameter systems.

For stoichiometric networks, the parameter system $\mathbf{p}=(\mathbf{h},\mathbf{j})$ has a single steady state for every (**h**,**j**). The domain of (**h**,**j**) is a convex polyhedral cone of dimension $n+r-d$. For these parameters the only restriction on (**h**,**j**) is $h_i \geqslant 0$ and $j_i \geqslant 0$. The situation is now very simple. The solutions of Eqs. (11) and (9) are the boundaries of regions where $\Delta_{d-1}(\mathbf{h},\mathbf{j})<0$ and $\alpha_d(\mathbf{h},\mathbf{j})<0$. We will call these *Hopf regions* and *saddle-node regions*, respectively. They are topologically equivalent to hyperspheres. When the regions do not overlap, the set of SN bifurcations is the boundary of all the SN regions, and the set of Hopf bifurcations is the boundary of all the Hopf regions.

When a pair of Hopf and SN regions overlap and the (**h**,**j**) parameters are used, the intersection of their boundaries is topologically equivalent to the surface of a codimension two hypersphere. The intersection consists of codimension two bifurcation points called Takens–Bogdanov (TB) points or double zero (DZ) points. Hale and Koçak[19] show possible dynamical phase diagrams near TB points in Figs. 13.8 and 13.9. The general treatment is given by Annabi *et al.*[4]

The rest of this section explains how the very simple global phase diagrams in the (**h**,**j**) parameters map into the conventional (**k**,**C**) parameters used experimentally. Figure 1 shows the typical intersection of Hopf and SN regions in the steady state manifold as parametrized by the (**h**,**j**) parameters. On phase diagrams throughout this paper, the Hopf region has the lightest shading (small dashed hatching), the SN region has medium shading (hatched

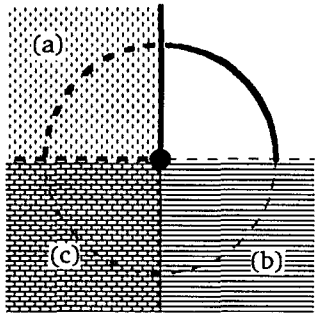

FIG. 1. Typical crossing of regions $\alpha_d<0$ and $\Delta_{d-1}<0$. The Hopf region (a) is reached by crossing a Hopf bifurcation from the stable region (upper right). The saddle node (SN) region (b) is reached by crossing a saddle-node bifurcation from the stable region. The two types of unstable regions overlap in region (c) which can be reached by crossing an SN^+ bifurcation from the Hopf region, or by crossing the symmetric eigenvalue curve from the SN region. The four regions meet at the Takens–Bogdanov point (large dot). The large circle shows how thick, thin, and dashed lines appear on a steady state manifold when it passes through the various regions.

lines), and their overlap has the darkest shading (brickwork pattern). The equation $\alpha_d=0$ is always a dashed line and $\Delta_{d-1}=0$ is always a solid line. The big dot at the center of Fig. 1 is a TB point. The boundary between the stable region in the upper right quadrant and the Hopf region is a thick solid line. The boundary between the stable region and the SN region is a thin dashed line. Thick solid and thin dashed lines represent Hopf and SN bifurcation hypersurfaces on all phase diagrams in this paper.

The dashed line $\alpha_d=0$ is the locus of a fold in the steady state manifold. The folding along this line is shown in Fig. 2, which is a 3-dimensional perspective of a concentration X plotted against typical rate constant parameters. When one of the steady states near the fold is stable an SN bifurcation occurs and the dashed line is thin. When

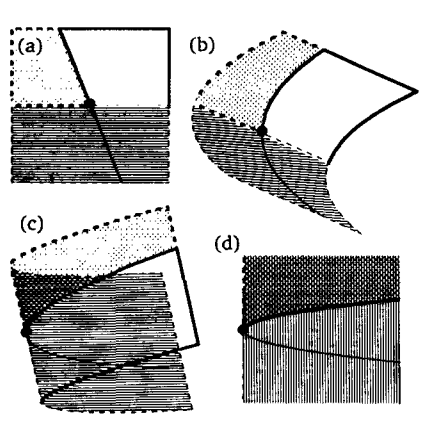

FIG. 2. Folding of the steady state manifold causes the picture in Fig. 1 to overlap itself. The flat steady state manifold in (a) is gradually folded with a perspective shift in (b), (c), and (d). View (d) is a phase diagram with SN and SN^+ bifurcation curves intersecting a TB point on the left side. The perimeter of the square in (a), which ends up as the top, right, and bottom edges of (d), is outlined with the types of lines used to draw curves on the steady state manifold.

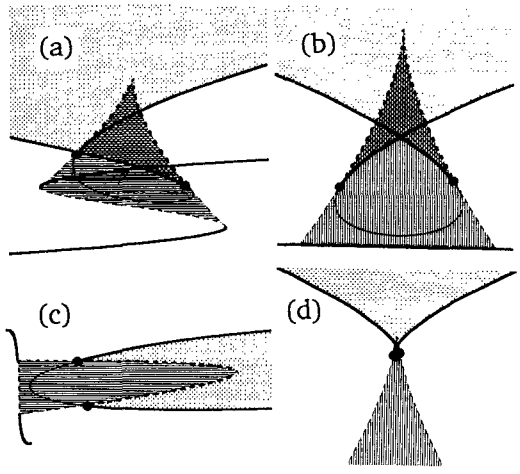

FIG. 3. Views of a Hopf bifurcation region overlapping with a saddle node cusp region. The foreground in (a) shows a typical S-shaped cross section through a steady state manifold in the region near a cusp. It is drawn using the line types used for curves on the steady state manifold. The background in (a) shows the shaded steady state manifold marked with bifurcation curves as in Fig. 2. The view from above (b) shows the resulting phase diagram. A side view is shown in (c). The curve in the steady state manifold of view (a) is shown edge on in view (b) and nearly edge on in (c). The typical cross-shaped phase diagram in (d) is (b) viewed from a distance.

neither is stable an SN^+ bifurcation occurs the dashed line is thick.

It is useful to plot the entire curve $\Delta_{d-1}=0$ on stoichiometric network phase diagrams to show the complete boundary of the Hopf regions. The curve that divides regions (b) and (c) in Fig. 1 does not represent a bifurcation. The curve's meaning can be discovered using Orlando's theorem. At the top of Fig. 1 the line $\Delta_{d-1}=0$ represents a pair of eigenvalues $\lambda=\pm i\omega$, whose sum vanishes. Moving downward along this line makes ω decrease to 0 at the TB (double zero) point. Moving further down, two real eigenvalues $\lambda=a$, $\lambda=-a$ appear and a increases. Since the eigenvalues are symmetrically placed on opposite sides of the imaginary axis, we call this curve the *symmetric eigenvalue* (SE) curve.

The SE curve has not been discussed previously. We believe it gives important insight into the global structure of phase diagrams for stoichiometric networks. Phase diagrams with many TB points must have Hopf curves that join the TB points in pairs. The same pairs are connected by SE curves. When a Hopf curve passes through the point at infinity the pair it connects may be unclear. In this case the SE curve shows which TB points belong to the pair.

Figure 2 shows that when folding is taken into account, the Hopf–SE and the SN–SN^+ curves are tangent at the TB point and do not cross.

Figure 3 shows how overlapping Hopf and SN regions produce the cross-shaped phase diagram frequently observed experimentally. When the Hopf region overlaps the cusp catastrophe associated with an S-shaped steady state manifold, two TB points are produced on opposite edges of the fold on each side of the cusp. These are joined by an SE curve which traverses the middle unstable steady state. The

TABLE I. Reaction mechanism of the Showalter–Noyes–Bar-Eli extended oregonator model.

R_1:	$BrO_3^- + Br^- + 2H^+ \rightleftharpoons HBrO_2 + HOBr$
R_2:	$HBrO_2 + Br^- + H^+ \rightleftharpoons 2HOBr$
R_3:	$BrO_3^- + HBrO_2 + H^+ \rightleftharpoons 2BrO_2 + H_2O$
R_4:	$Ce^{3+} + BrO_2 + H^+ \rightleftharpoons HBrO_2 + Ce^{4+}$
R_5:	$2HBrO_2 \rightleftharpoons BrO_3^- + HOBr + H^+$
R_6:	$Ce^{4+} \rightarrow gBr^- + Ce^{3+}$

SE and Hopf curves clearly show where $\Delta_{d-1} < 0$. The cross-shaped phase diagram appears when the details of Fig. 3 are compressed almost into a point.

Hopf and SN regions can overlap in two ways depending on whether the cusp of the $\alpha_d = 0$ curve lies inside or outside the Hopf region. In the first case (see Fig. 3) the cusp lies on the SN^+ curve and in the second it lies on the SN curve. The first case occurs in the SNB model. The second occurs in the Willamowski–Rossler network[20] and may be related to the chaos found in that model.

The Hopf, saddle node, and their overlap regions can be marked on plots of the steady state manifold using thick and thin dashed curves. The notation used throughout this paper is shown on the circle in Fig. 1.

IV. THE SHOWALTER–NOYES–BAR-ELI MODEL

Although the approach being developed is general, a concrete example will be used for clarity. This section shows the practical details of treating a moderately large network using the SNA software discussed elsewhere.[16]

The SNB model[8] of the BZ chemistry[21] is an extension of the well-known oregonator model of Field and Noyes.[7] The mechanism consists of the five reversible reactions and one irreversible reaction shown in Table I. These take place in a CSTR where BrO_3^-, Ce^{3+}, and Br^- enter with the flow and all species wash out. The model assumes $[H^+]$ is constant.

Reaction R_6 uses the parameter g to adjust the stoichiometry of Br^-. We replaced R_6 with two reactions corresponding to $g=0$ and $g=0.5$. Varying their relative rates is similar to varying g

$$R_{6.0}\colon\ Ce^{4+} \rightarrow Ce^{3+},$$

$$R_{6.5}\colon\ 2Ce^{4+} \rightarrow Br^- + 2Ce^{3+}.$$

If $k_{6.0} = (1-2g)k_6$ and $k_{6.5} = gk_6$ the combined rate and stoichiometry are the same as R_6. Ringland's calculations used $k_6 = 0.01\ s^{-1}$ and $g = 0.47$ and may be duplicated using $k_{6.0} = 0.0006\ s^{-1}$ and $k_{6.5} = 0.0047\ s^{-1}$.

The network diagram appears in Fig. 4. Reversible reactions are double lines whose head barbs and tail feathers indicate the stoichiometry and order of kinetics. For example, two tail feathers on $R_{6.5}$ indicate the stoichiometry is 2; one left feather indicates first order kinetics. Fixed species such as H^+ and pseudoreactions representing exchange with the CSTR reservoirs are marked with cup-shaped *reservoir symbols*. Reactions labeled with a reservoir symbols under a species name, such as Br^-, BrO_3^-, and Ce^{3+}, represent inflow of the species. The reverse reactions represent

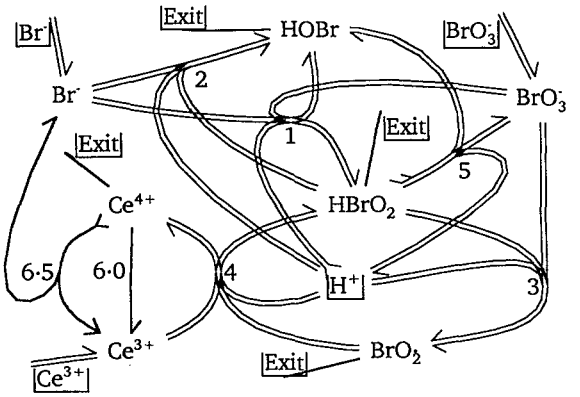

FIG. 4. Network diagram of SNB network.

outflow. Reactions with reservoir symbols marked "Exit" represent the outflow of other intermediates. All reservoir symbol reactions have rate constants proportional to the flow rate k_0.

The dynamics of the general network with power law kinetics is given by

$$\frac{d\mathbf{X}}{dt} = \mathsf{N}\,\mathrm{diag}(\mathbf{u})\mathrm{diag}(\mathbf{k})\mathbf{X}^{\mathsf{K}}, \tag{14}$$

where the stoichiometric and kinetic matrices $\mathsf{N}=(\nu_{ij})$ and $\mathsf{K}=(\kappa_{ij})$ have been introduced earlier. The vector $\mathbf{u}=(u_1,\cdots)$ enables us to include all reverse reactions in N and K and suppress the unused ones with $u_i=0$. In this notation, an n-component vector $\mathbf{X}$ raised to the power of an $n\times r$ matrix K is the r-component vector defined by

$$(\mathbf{X}^{\mathsf{K}})_k = \prod_{i=1}^{n} X_i^{\kappa_{ik}}.$$

To represent the SNB network in this form, the stoichiometric and kinetic matrices are split into blocks,

$$\mathsf{N} = (\mathsf{N}_R^+, \mathsf{N}_C^+, \mathsf{N}_R^-, \mathsf{N}_C^-),$$

$$\mathsf{K} = (\mathsf{K}_R^+, \mathsf{K}_C^+, \mathsf{K}_R^{-1}, \mathsf{K}_C^-),$$

$$\mathbf{u} = (\mathbf{u}_R^+, \mathbf{u}_C^+, \mathbf{u}_R^-, \mathbf{u}_C^-),$$

where the superscripts + and − refer to forward and reverse reactions, the subscript R refers to real reactions $R_1,\ldots,R_{6.5}$, and the subscript C refers to CSTR pseudoreactions. Then $\mathsf{N}_R^- = -\mathsf{N}_R^+$, and the forward stoichiometric matrix N_R^+ is

$$\begin{array}{c} \\ \mathrm{A}(BrO_3^-) \\ \mathrm{Y}(Br^-) \\ \mathrm{W}(Ce^{3+}) \\ \mathrm{Z}(Ce^{4+}) \\ \mathrm{X}(HBrO_2) \\ \mathrm{U}(BrO_2) \\ \mathrm{P}(HOBr) \end{array} \begin{array}{c} \begin{array}{ccccccc} R_1 & R_2 & R_3 & R_4 & R_5 & R_{6.0} & R_{6.5} \end{array} \\ \left(\begin{array}{ccccccc} -1 & 0 & -1 & 0 & 1 & 0 & 0 \\ -1 & -1 & 0 & 0 & 0 & 0 & 1 \\ 0 & 0 & 0 & -1 & 0 & 1 & 2 \\ 0 & 0 & 0 & 1 & 0 & -1 & -2 \\ 1 & -1 & -1 & 1 & -2 & 0 & 0 \\ 0 & 0 & 2 & -1 & 0 & 0 & 0 \\ 1 & 2 & 0 & 0 & 1 & 0 & 0 \end{array}\right) \end{array}. \tag{15}$$

At the left is an alternative notation for the intermediates, such as A for BrO_3^-, which will be needed later. The CSTR pseudoreaction stoichiometric matrices are

$$N_C^+ = -N_C^- = \mathrm{diag}(1,1,1,-1,-1,-1,-1).$$

Unused reverse reactions are suppressed by

$$u_R^- = (1,1,1,1,1,0,0), \quad u_C^- = (1,1,1,0,0,0,0).$$

The orders of kinetics for the forward and reverse of the real reactions are given by the transposes of the kinetic matrices for the real reactions and diagonal matrices for the CSTR reactions

$$(K_R^{+t}, K_R^{-t}) = \begin{array}{c} \\ R_1 \\ R_2 \\ R_3 \\ R_4 \\ R_5 \\ R_{6.0} \\ R_{6.5} \end{array} \begin{pmatrix} 1 & 1 & 0 & 0 & 0 & 0 & 0 & 0 & 0 & 0 & 0 & 1 & 0 & 1 \\ 0 & 1 & 0 & 0 & 1 & 0 & 0 & 0 & 0 & 0 & 0 & 0 & 0 & 2 \\ 1 & 0 & 0 & 0 & 1 & 0 & 0 & 0 & 0 & 0 & 0 & 0 & 2 & 0 \\ 0 & 0 & 1 & 0 & 0 & 1 & 0 & 0 & 0 & 0 & 1 & 1 & 0 & 0 \\ 0 & 0 & 0 & 0 & 2 & 0 & 0 & 1 & 0 & 0 & 0 & 0 & 0 & 1 \\ 0 & 0 & 0 & 1 & 0 & 0 & 0 & 0 & 0 & 1 & 0 & 0 & 0 & 0 \\ 0 & 0 & 0 & 1 & 0 & 0 & 0 & 0 & 1 & 2 & 0 & 0 & 0 & 0 \end{pmatrix},$$

$$K_C^+ = \mathrm{diag}(0,0,0,1,1,1,1), \quad K_C^- = \mathrm{diag}(1,1,1,0,0,0,0).$$

N and K are 7×28, however, only 22 reactions are actually used. The advantage of combining reactions and pseudoreactions into such large matrices is that simple Eq. (14) may be used to develop the theory.

Our principle objective is to derive approximate equations for the bifurcation hypersurfaces of networks. In order to check the approximations used in the analytical treatment we developed software that traces the steady state manifold and phase diagram curves numerically using continuation methods developed by Kubicek.[22] The software works for any stoichiometric network. A typical steady state manifold of the SNB network (using the same rate constants as Ringland) is shown in Fig. 5. The stability at each point on the curve was determined by evaluating the first row of the Routh array numerically and is shown using the line-type conventions in Figs. 1–3. The bifurcation points marked (a)–(d) will play a key role in deriving equations later. Figure 6 shows a phase diagram consisting of two curves $\Delta_{d-1}=0$ and $\alpha_d=0$. The shading emphasizes the similarity to Fig. 3. Of particular interest is the symmetric eigenvalue curve which joins the two TB points.

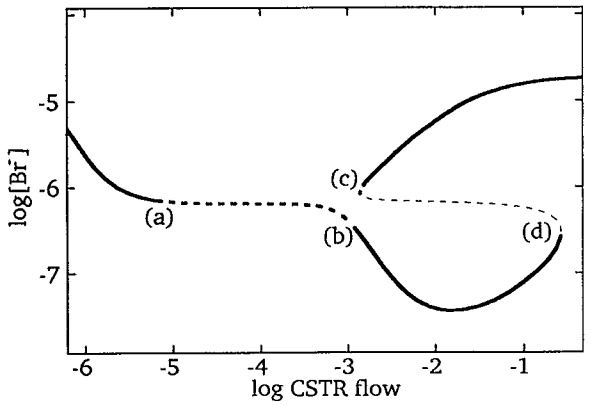

FIG. 5. Steady state manifold of SNB network. The line types follow the scheme in the large circle of Fig. 1. A Hopf region occurs between (a) and (b). SN^+ and Hopf bifurcations occur very close together at (c) and (d). The parameters for this cross section are $[Br^-]_0=2.0\times10^{-5}$ M, $[BrO_3^-]_0=0.14$ M, $[Ce^{3+}]_0=8.3\times10^{-4}$ M, $[H^+]=1.0$ M, $k_1=8.4\times10^{-2}$ $M^{-1}s^{-1}$, $k_{-1}=1.0\times10^4$ $M^{-1}s^{-1}$, $k_2=4.0\times10^8$ $M^{-2}s^{-1}$, $k_{-2}=5.0\times10^{-5}$ $M^{-1}s^{-1}$, $k_3=2.0\times10^3$ $M^{-2}s^{-1}$, $k_{-3}=2.0\times10^7$ $M^{-1}s^{-1}$, $k_4=1.3\times10^5$ $M^{-2}s^{-1}$, $k_{-4}=2.4\times10^7$ $M^{-1}s^{-1}$, $k_5=4.0\times10^7$ $M^{-1}s^{-1}$, $k_{-5}=4.0\times10^{-11}$ $M^{-2}s^{-1}$, $k_{6.0}=6.0\times10^{-4}s^{-1}$, $k_{6.5}=4.7\times10^{-3}s^{-1}$.

V. PARAMETERS FOR THE ANALYTICAL STABILITY ANALYSIS

When we later derive equations for most of the curves shown in Fig. 3, the analysis will be carried out using $(\mathbf{h},\mathbf{j})$ parameters and then converted to rate constants and flow rates. We begin with a general discussion of the numbers of parameters required and the conditions which the parameters must satisfy. Starting with an initial set of 22 parameters, these conditions make some parameters dependent on others and reduce the number of truly independent pa-

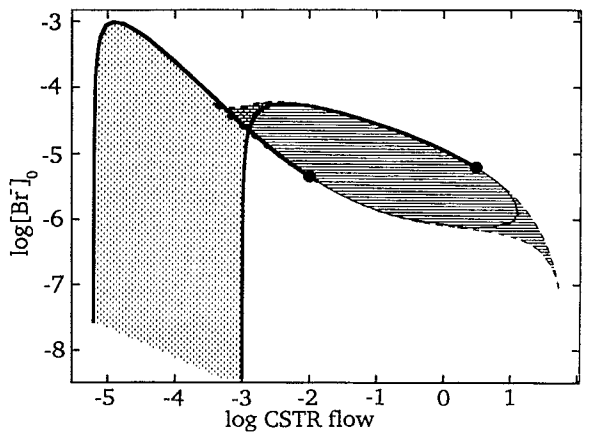

FIG. 6. Phase diagram of SNB network. The Hopf region (left) and saddle node region (right) overlap as in Fig. 3(b).

rameters to 13. We show that the reduction from 22 to 13 parameters occurs for both the (**k**,**C**) and (**h**,**j**) parameters.

The stoichiometric matrix N has 14 columns each for forward and reverse reactions. Since 6 reverse reactions are unused there are 22 rate constants or **k** parameters. The full set of (**k**,**C**) parameters consists of just these rate constants because no conservation conditions are present (**C** is a 0-dimensional vector). Twelve of the **k** parameters are for real reactions, and ten are for reservoir pseudoreactions. Six of these ten may be eliminated by recognizing that they are determined by four parameters: the flow rate k_0, and the three input concentrations of Br^-, BrO_3^-, and Ce^{3+}. The *CSTR constraints* make six of these ten rate constants dependent on the other four. The remaining 16 parameters are not all independent because three reactions add up to a null reaction

$$R_1+R_{-2}+R_5=0, \tag{16}$$

which implies the equilibrium constants satisfy

$$K_1K_2^{-1}K_5=1,$$

and the rate constants obey a *Wegscheider condition*[23]

$$k_1k_{-2}k_5=k_{-1}k_2k_{-5}. \tag{17}$$

Thus only 15 parameters are truly independent. Since the phase diagram is unchanged if the concentrations and time are rescaled, two more parameters may be eliminated using dimensionless parameters. The phase diagram depends on 13 true independent parameters. Some of these are the rate constants of reactions which have no effect on the phase diagram in the region of experimental interest. Eliminating unimportant reactions can reduce the dimension of the phase diagram further.

When the network is analyzed with SNA, there are 22 (**h**,**j**) parameters that are equivalent to the 22 (**k**,**C**) parameters, and 13 true independent (**h**,**j**) parameters. The 22 (**h**,**j**) parameters consist of 7 **h** parameters, which are the reciprocal steady state concentrations of the intermediates, and 15 **j** parameters, which are the rates of certain sets of extreme currents, or for brevity "currents."[24] The general network has n **h** parameters and $(r-d)$ **j** parameters. How the CSTR constraints make six of these parameters dependent requires an explanation. In a CSTR, the **h** parameters of intermediates that wash out are determined by the rates of currents washing them out. Let exit(X) be the set of currents washing out intermediate X via exit reaction R_i. The **h** parameter for X is given by the CSTR constraint equation

$$h_X=\frac{1}{[X]}=k_0/\left(\sum_{k\in\text{exit}(X)} E_{ik}\,j_k\right). \tag{18}$$

Since this introduces the parameter k_0 and removes 7 **h** parameters, the number of parameters decreases from 22 to 16.

The elimination of two more parameters to produce dimensionless variables is simple using (**h**,**j**) parameters. The matrix M in Eq. (3) is homogeneous in both **h** and **j**. Hence, one may obtain dimensionless parameters by dividing all **h** parameters by one of them and all **j** parameters by one of them. Another approach is to set $h_1=1$ and $j_1=1$ and interpret the parameters relative to these two. Nothing is gained because the polynomials α_d and Δ_{d-1} have the same number of terms. The analysis is just as easy without dimensionless parameters and the final equations are easier to interpret.

If the reduction to dimensionless parameters is applied by setting $h_1=1$ and the CSTR constraint Eq. (18) is applied next, the constraint for the first species is

$$k_0=\sum_{k\in\text{exit}(X)} E_{ik}\,j_k.$$

Thus k_0 is determined by the independent parameters which are 14 ratios of currents.

The Wegscheider condition reduces the number of independent current ratios to 13. Multiply Eq. (17) on both side by suitable powers of concentration to get

$$v_1v_{-2}v_5=v_{-1}v_2v_{-5}. \tag{19}$$

This equation holds for all concentrations including steady state where Eq. (4) applies. Thus

$$(\mathbf{E}_1\cdot\mathbf{j})(\mathbf{E}_{-2}\cdot\mathbf{j})(\mathbf{E}_5\cdot\mathbf{j})=(\mathbf{E}_{-1}\cdot\mathbf{j})(\mathbf{E}_2\cdot\mathbf{j})(\mathbf{E}_{-5}\cdot\mathbf{j}), \tag{20}$$

where $\mathbf{E}_i$ is the ith row of E. This constraint makes one current ratio dependent.

When $k_0=0$ and the system is closed, Wegscheider's condition forbids currents which cycle around $R_1+R_{-2}+R_5$ or the reverse. To see why, note that the detailed balanced currents produce identical terms on both sides of Eq. (20). A nondetailed balanced cycling current that represents a net flow around the cycle would add terms to only one side of the equation. These terms must vanish to make both sides equal. Hence a net flow around the cycle is forbidden in the closed system. When $k_0=0$ and the system is open, nondetailed balanced steady states are possible provided terms are added to both sides of Eq. (20). This equation makes one **j** parameter dependent on the others so the number of true independent (**h**,**j**) parameters is 13.

VI. FINDING THE IMPORTANT REACTIONS AND CURRENTS

Our aim is to extract approximate equations for the curves on the phase diagram. If an exact analysis using all 13 true independent parameters were carried out, probably only a few parameters would be important in the equation satisfied by a bifurcation point. The remaining parameters would be negligible terms if they appeared in the curve's equation.

The best approach eliminates insignificant parameters from the original 22 parameters first and constructs the true independent parameters later. The eliminated parameters can be regarded as the rate constants of unimportant reactions, or the rates j_i of unimportant currents. In this section we take the latter viewpoint because when the SNA software derives equations for bifurcation curves it uses (**h**,**j**) parameters. We develop a systemmatic method of

ranking the currents in importance near an arbitrary bifurcation point so that the least important currents can be omitted.

How the network is simplified is the key to whether or not it will be possible to get simple equations in the rate constants. There are two important issues. First, there are many ways to choose a set of currents matching given $(\mathbf{k},\mathbf{C})$ parameters. The set must be chosen carefully. A suitable method is described below. Second, the currents that can be omitted are not necessarily those with the smallest j_i's. How essential currents are chosen will be discussed.

We begin with a review of basic ideas concerning currents. For a more detailed discussion see Ref. 25. The set of steady state rate vectors $\mathbf{v}$ is the intersection of the 15-dimensional right null space of N and the non-negative orthant defined by $v_i \geqslant 0$ for all R_i. This set is a convex polyhedral current cone which can be shown to have 53 edges. The current matrix E has 53 columns, which are vectors in the corresponding edges. Since the cone is 15-dimensional, 15 currents can be chosen as a basis and any steady state $\mathbf{v}$ may be expressed as a linear combination of them. The coefficients $\mathbf{j}$ are the rates of the currents. Negative rates are meaningless so we require all $j_i \geqslant 0$. No single set of basis currents has non-negative j_i for all steady states $\mathbf{v}$. Hence, different sets of basis currents must be used with different $\mathbf{v}$'s. Each steady state $\mathbf{v}$ can then be represented as $\mathbf{v}=\mathsf{E}\mathbf{j}$, where $j_i \geqslant 0$ for the 15 basis currents, and $j_i=0$ otherwise. The sets of basis currents are not unique and are called *selected currents.*

Consider the possible consequences of approximating a network by deleting a reaction. The number of reactions changes from r to $(r-1)$ and the rank of N either remains d or changes to $(d-1)$. In the first case the dimension of the current cone decreases from $(r-d)$ to $(r-1-d)$, which is 14. One fewer basis current is required to represent $\mathbf{v}$. In the second case the number of basis currents does not change, but the number of conservation conditions increases from $(n-d)$ to $(n-d+1)$, which is 1. Thus deleting a reaction either decreases the basis to 14 currents or creates a conservation condition. The latter occurs when an intermediate becomes isolated and its concentration is fixed by a conservation condition. In the highly interconnected SNB model, deleting most reactions reduces the dimension of the current cone. If reactions are deleted successively, the first deletions usually reduce the dimension. Later deletions are more likely to create conservation conditions because the probability of isolating a species increases as the network becomes less interconnected.

When R_i is deleted, no current that uses R_i can occur. If only one current $\mathbf{E}_k$ of the 15 selected currents uses the deleted reaction R_i, the remaining 14 currents are currents of the network of the remaining reactions. These may be used to represent $\mathbf{v}$ with $\mathbf{j} \geqslant 0$ in the approximate network. In this situation the ith row of the original E contains only one nonzero entry E_{ik} among the 15 columns of the selected currents and $v_i = E_{ik} j_k$. Since E_{ik} is a small integer, the reaction and current rates have the same order of magnitude.

This pairing between reactions and currents can be used to rank them in order of importance. To make the method work, the algorithm that selects currents must be designed so the set of remaining currents after deleting the smallest current at any stage is a valid set of selected currents for the network which remains. Then currents can be deleted from the smallest to the largest to obtain a series of approximate networks.

The algorithm for selecting currents must be the reverse of the deletion procedure. Starting from a given steady state $\mathbf{v}$, calculate the largest j_k for each current $\mathbf{E}_k$ that satisfies

$$\mathbf{v}-\mathbf{E}_k j_k \geqslant 0.$$

Select the current with the largest j_k. The algorithm is easier to describe if this current is called $\mathbf{E}_1$. Subtract $\mathbf{E}_1 j_1$ from $\mathbf{v}$ to get the first residue

$$\mathbf{v}^{(1)} = \mathbf{v} - \mathbf{E}_1 j_1.$$

Note that one component v_i (say) of $\mathbf{v}^{(1)}$ must be 0 or else j_1 could have been made bigger. Then recalculating $\mathbf{k}$ from

$$\mathbf{k} = \mathrm{diag}(\mathbf{v})\mathbf{h}^{\mathsf{K}},$$

gives $k_i=0$. Thus $\mathbf{v}^{(1)}$ is a steady state of a subnetwork with R_i deleted. Next repeat the process for this subnetwork, and iterate. If the currents are numbered so the selected currents in successive iterations are $\mathbf{E}_2,\mathbf{E}_3,\ldots,\mathbf{E}_{15}$, the residue after 15 iterations is

$$\mathbf{v}^{(15)} = \mathbf{v} - \mathbf{E}_1 j_1 - \mathbf{E}_2 j_2 - \cdots - \mathbf{E}_{15} j_{15}.$$

The residue is a steady state of the network which results from deleting reactions at each stage. Each iteration reduces the dimension of the null space of N by one, so after 15 iterations the dimension is 0 and the only steady state is $\mathbf{v}^{(15)}=0$. Hence

$$\mathbf{v} = \mathbf{E}_1 j_1 + \mathbf{E}_2 j_2 + \cdots + \mathbf{E}_{15} j_{15}. \tag{21}$$

When $\mathbf{E}_1,\ldots,\mathbf{E}_{15}$ are the selected currents, $\mathbf{v}$ has coefficients $j_1,\ldots,j_{15}$ which get smaller in the sequence $j_1 > j_2 > \cdots > j_{15}$. When currents are deleted in the reverse order $\mathbf{E}_{15},\ldots,\mathbf{E}_1$, those which remain at each stage are a suitable set of selected currents for the remaining network at that stage.

This method was used to select and rank currents close to the bifurcation points marked (a), (b), (c), and (d) on the steady state manifold in Fig. 5. For each point, the ranking for currents in steady states on both sides are given in Table II. Note that crossing a bifurcation causes small changes in the sequence of the currents. Since equations in the $(\mathbf{h},\mathbf{j})$ parameters for the bifurcation curves frequently state that two currents are equal, currents which switch sequence are likely to be appear in the bifurcation curve equation.

Because the smaller currents $\mathbf{E}_k$ correspond to a unique reaction R_i, and j_k and v_i are the same order of magnitude, the least important reactions can be read from the table. For example, the rate of $\mathbf{E}_5$ is the rate of R_{-5} and its ranking at the bottom for three of the bifurcation points tells us the reverse of R_5 is never important. Removing this

TABLE II. Currents in descending order of importance on the stable (S) and unstable (U) side of Hopf bifurcation points, for high (H), middle (M), and low (L) steady states near SN^+ bifurcation points, and at the low-flow Takens–Bogdanov point (TB). Essential currents are marked.

Left Hopf		Right Hopf		Left SN^+		Right SN^+		TB
S	U	S	U	H	M	L	M	
7	7	7	7	*7	*7	*7	*7	*7
*12	*12	4	4	*8	*8	*8	*8	*8
*4	*4	*8	*8	12	4	*4	*4	*51
*1	8	*3	*12	4	12	*3	*51	*15
8	*1	*12	*3	*15	*51	*51	*3	*12
2	2	*20	*20	*51	*15	12	12	6
21	21	52	52	52	52	39	23	*4
52	52	1	21	6	6	23	6	52
3	20	21	1	21	21	6	39	21
20	3	40	40	3	3	20	22	3
6	6	6	6	25	25	24	21	25
40	40	25	25	40	40	1	1	24
5	5	2	2	2	2	22	20	40
25	25	24	24	24	24	2	2	2
24	24	5	5	5	5	5	5	5

reaction makes the Wegscheider condition inapplicable. Other unimportant reactions in order of increasing significance are the exit of $HBrO_2$ and BrO_2 from the CSTR, the reverse reaction R_{-2}, and the exit of Br^-.

Before deriving bifurcation curves we must omit as many parameters as possible such that the bifurcation point is still present in the simplified network. The currents which remain are the *essential currents* of the bifurcation point. This step requires SNA software that is capable of analyzing a network in a few seconds to determine the effects of approximations. The procedure makes use of the program's ability to switch back and forth between (**h,j**) and (**k,C**) parameters.

The curve in Fig. 5 is first displayed using the full set of (**h,j**) parameters and with (**h,j**) having the numerical values at one of the bifurcation points (a)–(d). We then set certain $j_i=0$ and recalculate Fig. 5 to see if the bifurcation point still exists. The approximation may totally change the appearance of the rest of the curve, but only the region of the bifurcation point matters. Repeated testing produces the minimal set of currents needed for the existence of the bifurcation point.

These approximations are not equivalent to deleting a reaction and using all remaining reactions with the original rate constants. Setting $j_i=0$ usually changes all rate constants when (**k,C**) is recalculated from (**h,j**). Since the Jacobian matrix M is a simple function of (**h,j**), eliminating the smallest currents removes the smallest terms in M. The effect on M is minimal, and the location of the bifurcation changes as little as possible.

Essential currents are marked in Table II with asterisks. Three essential currents $\mathbf{E}_1$, $\mathbf{E}_3$, and $\mathbf{E}_4$ are the detailed balance cycling rates of reactions R_1, R_3, and R_4. The remaining essential currents contribute the following submatrix to the transpose of E:

	R_1	R_2	R_3	R_4	$R_{6.5}$	C_A	C_Y	C_W	C_{-Z}	C_{-P}	R_{-1}	C_{-A}	C_{-W}
$\mathbf{E}_7$	0	0	0	0	0	1	0	0	0	0	0	1	0
$\mathbf{E}_8$	0	0	0	0	0	0	0	1	0	0	0	0	1
$\mathbf{E}_{12}$	0	1	1	2	1	1	0	0	0	2	0	0	0
$\mathbf{E}_{15}$	1	1	0	0	0	1	2	0	0	3	0	0	0
$\mathbf{E}_{20}$	0	1	2	4	0	1	0	4	4	1	1	0	0
$\mathbf{E}_{51}$	0	1	1	2	0	1	1	2	2	2	0	0	0

The columns labeled C_i and C_{-i} are CSTR input and output reactions. The symbols used for the intermediates were given in Eq. (15). Thus C_A, C_{-A}, C_Y, C_{-Y}, C_W, and C_{-W} are the inputs and outputs of $A(BrO_3^-)$, $Y(Br^-)$, and $W(Ce^{+3})$. C_{-Z} and C_{-P} are outputs of $Z(Ce^{+4})$ and P(HOBr). Reactions not appearing are not important.

These essential reactions form a network with ten true independent parameters, however, even simpler networks will be used near each bifurcation point.

VII. THE LOW-FLOW HOPF BIFURCATION CURVE

In this section we derive the equation of the vertical Hopf bifurcation curve at the far left in Fig. 6. The intui-

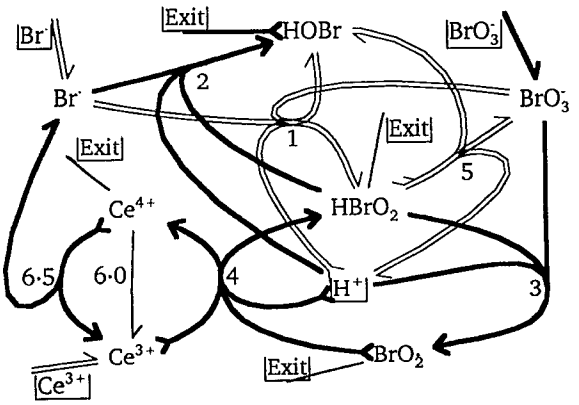

FIG. 7. Extreme current $\mathbf{E}_{12}$ destabilizes in the Hopf region.

tive physical understanding of the significant terms in the equations is probably as important as the equation itself.

The low-flow Hopf bifurcation has three essential currents $\mathbf{E}_{12}$, $\mathbf{E}_4$, and $\mathbf{E}_1$. The largest current $\mathbf{E}_7$ is not essential. It is a *flow-through current* that represents the entrance and exit of BrO_3^- from the CSTR. When its rate is large enough $[BrO_3^-] \approx [BrO_3^-]_0$. The fact that this current is not essential indicates the destabilizing feedback cycle does not involve BrO_3^- and the clamping effect of this current on $[BrO_3^-]$ does not affect the stability.

Essential currents $\mathbf{E}_1$ and $\mathbf{E}_4$ represent the detailed balanced cycling in R_1 and R_4 at equilibrium. Every intermediate appears in these two reactions, and if we were treating an equilibrium state, R_1 and R_4 would determine all the concentrations at equilibrium.

A stability analysis with three currents took 2.5 min[26] to derive four systems of 60 inequalities using symbolic algebra. The important system contains

$$\begin{aligned} &j_{12} > 3j_1, \\ &[BrO_3^-] > [Br^-], \\ &j_{12}[Ce^{4+}] > 2j_1[Br^-], \\ &j_{12}[HOBr] > 2j_1[Br^-]. \end{aligned} \tag{22}$$

The steady state is unstable when all of these are satisfied.

Current $\mathbf{E}_{12}$ (see Fig. 7) is unstable. Starting at a very low flow rate and increasing k_0, a Hopf bifurcation occurs when j_{12} becomes greater than three times the rate of the equilibrium current $\mathbf{E}_1$. This happens in the ranking of Table II. How is j_{12} connected to flow rate? Note that $j_{12} = v_3 \propto [BrO_3^-]$. As the flow rate increases, $[BrO_3^-]$ increases from the low equilibrium level determined by R_1 and R_4 to the value $[BrO_3^-]_0$ produced by the clamping effect of $\mathbf{E}_7$. Increasing the flow rate increases $[BrO_3^-]$ and consequently j_{12} until $j_{12} = 3j_1$, where a Hopf bifurcation occurs. The bifurcation curve is a vertical line on the phase diagram because $[Br^-]_0$ only affects the stability if it raises $[Br^-]$ enough to violate one of the inequalites. This only happens near the top of Fig. 6. At lower $[Br^-]_0$ the last three inequalities of Eq. (22) are satisfied and not close to being equalities.

Even though current $\mathbf{E}_7$ was not needed to get Eqs. (22), it is needed to get the correct dependence of $[BrO_3^-]$ on flow rate. For currents $\mathbf{E}_1$, $\mathbf{E}_4$, $\mathbf{E}_7$, and $\mathbf{E}_{12}$ the Hopf bifurcation flow rate condition $j_{12} = 3j_1$ is equivalent to

$$k_0 = \frac{108 k_1 k_{-1}^2 [H^+][BrO_3^-]_0}{k_2(6k_{-1} + k_3[H^+])}. \tag{23}$$

This formula gives the flow rate of the vertical Hopf bifurcation line on Fig. 6. The derivation uses a general approach which will be explained in detail for this example. Use Eq. (4) and express each reaction rate using its rate law

$$v_1 = k_1 H^2 AY = j_1, \tag{24.1}$$

$$v_{-1} = k_{-1} PX = j_1, \tag{24.2}$$

$$v_2 = k_2 HXY = j_{12}, \tag{24.3}$$

$$v_3 = k_3 HAX = j_{12}, \tag{24.4}$$

$$v_4 = k_4 HUW = j_4 + 2j_{12}, \tag{24.5}$$

$$v_{-4} = k_{-4} XZ = j_4, \tag{24.6}$$

$$v_{6.5} = k_{6.5} Z = j_{12}, \tag{24.7}$$

$$v_A = k_0 A_0 = j_{12} + j_7, \tag{24.8}$$

$$v_{-A} = k_0 A = j_7, \tag{24.9}$$

$$v_{-P} = k_0 P = 2j_{12}. \tag{24.10}$$

The approximate network requires the conservation condition $W + Z = C$ as an 11th equation. These equations determine the seven intermediate concentrations and four currents. In principle, these equations could be solved and substituted into $j_{12} = 3j_1$ to get Eq. (23). However, it is much easier to append the bifurcation condition as a 12th equation and extract the relationship among the parameters directly. Taking this approach, we eliminate j_{12} using $j_{12} = 3j_1$, j_4 using Eq. (24.6), and j_7 using Eq. (24.9) to get

$$v_1 = k_1 H^2 AY = j_1, \tag{25.1}$$

$$v_{-1} = k_{-1} PX = j_1, \tag{25.2}$$

$$v_2 = k_2 HXY = 3j_1, \tag{25.3}$$

$$v_3 = k_3 HAX = 3j_1, \tag{25.4}$$

$$v_4 = k_4 HUW = k_{-4} XZ + 6j_1, \tag{25.5}$$

$$v_{6.5} = k_{6.5} Z = 3j_1, \tag{25.6}$$

$$v_A = k_0 A_0 = 3j_1 + k_0 A_0, \tag{25.7}$$

$$v_{-P} = k_0 P = 6j_1. \tag{25.8}$$

These nine equations (including $W + Z = C$) in seven concentrations and j_1 can only be satisfied if there is one relationship among the parameters. It can be obtained in three steps. Eliminate j_1 from Eqs. (25.2) and (25.8), and eliminate j_1 from Eqs. (25.1) and (25.3) to get

$$X = k_0 / 6k_{-1},$$

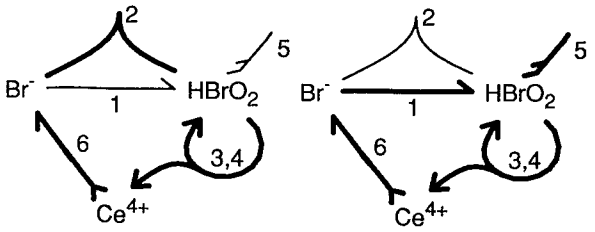

FIG. 8. The irreversible oregonator has two extreme currents. The left current is unstable and the right current is stable. Reaction numbering has been altered to correspond to the SNB model.

$$A = k_0 k_2 / 18 H k_1 k_{-1}.$$

Use Eq. (25.4) to replace $3j_1$ in Eq. (25.7) to get

$$k_0 A_0 = k_3 \mathrm{HAX} + k_0 A_0$$

Substituting for X and A and solving for k_0 yields Eq. (23).

This method does not eliminate the need for algebra; however, knowing the bifurcation condition before solving for the steady states greatly simplifies the algebra. If it is possible to derive an equation for the bifurcation curve, this method is most likely to succeed because a clear intuitive understanding of the instability can lead directly to the best approximations.

VIII. COMPARISON WITH THE OREGONATOR

The Hopf region in the lower left of Fig. 6 is caused by the same reactions and feedback cycles that produce oscillations and Hopf bifurcations in the oregonator.[7] The irreversible oregonator has two extreme currents which are shown in Fig. 8. The right-hand current is stabilizing. The left-hand current has a destabilizing positive feedback cycle which involves two network features. First, $HBrO_2$ lies on a critical current cycle that involves reactions R_3 and R_4. Second, $HBrO_2$ lies on a positive feedback 2-cycle involving Br^- which occurs because both are reactants of R_2. Theorem V.10 in Ref. 10 explains how this instability arises. It is a prototype in the instability classification scheme of Eiswirth, Freund, and Ross.[27]

This destabilizing oregonator current closely resembles $\mathbf{E}_{12}$ in Fig. 7 of the SNB model. Both contain the key destabilizing reactions $\mathbf{R}_2$, $\mathbf{R}_3$, and $\mathbf{R}_4$, the critical current cycle, and the positive feedback cycle between $HBrO_2$ and Br^-.

The SNB low-flow Hopf bifurcation is a balance between this instability and the stability of near-equilibrium steady states. The key is whether a perturbation that increases $[HBrO_2]$ above steady state is followed by a return to steady state or a further increase. On the high-flow side, the positive feedback cycle causes an increase. On the low-flow side, R_1 shifts to decrease $HBrO_2$ by Le Chatelier's principle. Thus the rate constants that should affect the location of the Hopf bifurcation are k_1, k_{-1}, k_2, and k_3. These are precisely the rate constants in Eq. (23)

The oregonator can be stabilized by the right-hand current in Fig. 8; however, this current requires R_5 which does not occur in any of the essential currents of Table II.

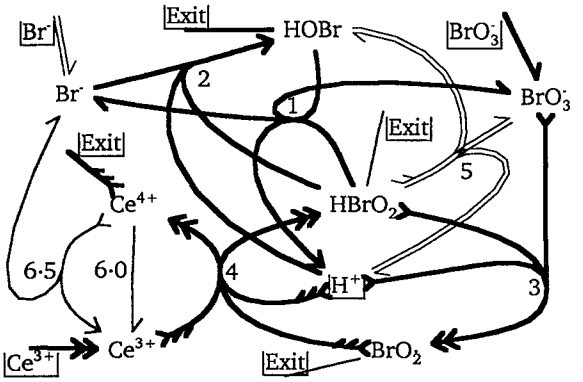

FIG. 9. Extreme current $\mathbf{E}_{20}$ stabilizes the high-flow Hopf bifurcation. This current only becomes significant when the flow rate is large enough to wash out Ce^{4+}.

IX. THE HIGH-FLOW HOPF BIFURCATION CURVE

The key ideas will be presented and then the detailed analysis. The oregonator can be stabilized by increasing detailed balance cycling in R_3. When stabilization occurs by this mechanism, a perturbation that increases $[HBrO_2]$ is followed by a decrease from a Le Chatelier shift in R_3 instead of an increase from the positive feedback cycle involving R_2. This can only happen when the detailed balance current in R_3 is significant. For the SNB network, Table II shows this current is one of the largest and becomes even larger when the high-flow Hopf bifurcation is crossed from instability to stability.

Why does detailed balance cycling in R_3 become more significant as the flow rate increases? The higher flow rate washes Ce^{4+} out of the CSTR in current $\mathbf{E}_{20}$ shown in Fig. 9. Since Ce^{4+} does not produce Br^-, reaction R_2 cannot remove $HBrO_2$ fast enough and detailed balanced currents become more important in R_3 and R_4.

To develop this picture we proceed systematically as in the low-flow Hopf bifurcation case. Table II shows unstable current $\mathbf{E}_{12}$ is stabilized by currents $\mathbf{E}_3$, $\mathbf{E}_8$, and $\mathbf{E}_{20}$. All four are essential currents. $\mathbf{E}_3$ is the detailed balance cycling in R_3 which can stabilize the oregonator. $\mathbf{E}_8$ is the flow-through current for Ce^{3+}.

A stability analysis using the four essential currents produced ten systems of 237 inequalities. Of these, we discuss

$$\begin{aligned} &j_{12} > j_3, \\ &j_{12} > 3j_{20}, \\ &[BrO_3^-] > [Br^-], \\ &j_{12}[Ce^{4+}] > j_3[Br^-], \end{aligned} \tag{27}$$

which must all be satisfied for instability in the region of interest. The ranking of the currents in Table II shows that $j_{12} = j_3$ and possibly $j_{12} = 3j_{20}$ at the Hopf bifurcation.

For the approximate network consisting of the essential currents plus $\mathbf{E}_7$, the steady state concentrations along a bifurcation curve such as $j_{12} = 3j_{20}$ or $j_{12} = j_3$ are easier to solve than in the general case. The bifurcation curves do

not depend on $[Br^-]_0$ because the input reaction is not included in the approximate network. The bifurcation curve $j_{12}=3j_{20}$ is equivalent to the following condition on the flow rate

$$k_0=\tfrac{4}{3}k_{6.5}. \tag{28}$$

To derive this, note that in current $\mathbf{E}_{20}$ Ce^{4+} washes out with rate $4j_{20}$, and this occurs when $[Ce^{4+}]=4j_{20}/k_0$. In current $\mathbf{E}_{12}$ Ce^{4+} reacts with $R_{6.5}$ with rate j_{12}, and this occurs when $[Ce^{4+}]=j_{12}/k_{6.5}$. The two expressions for $[Ce^{4+}]$ must be equal so $4j_{20}/k_0=j_{12}/k_{6.5}$. Then Eq. (28) follows from the bifurcation curve equation $j_{12}=3j_{20}$.

Condition (28) has a simple intuitive meaning. Stabilization occurs at the flow rate where a significant amount of Ce^{4+} washes out of the CSTR. A larger value of $k_{6.5}$ makes $R_{6.5}$ consume more Ce^{4+} lowering its steady state concentration. A proportionally larger flow rate is required to make significant amounts of Ce^{4+} wash out.

Comparison of Eq. (28) with $k_{6.5}=0.0047\ s^{-1}$ and the data in Fig. 6 of Ringland's paper shows that the experimental bifurcation occurs at roughly 1.5 times the maximum possible rate given by Eq. (28). To fit the experiments $k_{6.5}$ must increase and k_3 and k_{-3} must decrease so detailed balanced cycling in R_3 does not stabilize the oscillations at too low a flow rate.

X. THE REGION OF MULTIPLE STEADY STATES

The region of multiple steady states, or SN region (see Fig. 6), is bounded by the SN and SN^+ curve on the phase diagram. The boundaries on the upper right and lower left are very roughly linear with slope -1. Thus

$$\log[Br^-]_0+\log k_0=\text{constant},$$

$$k_0[Br^-]_0=\text{constant},$$

Since Br^- is supplied to the CSTR at the constant rate k_0 $[Br^-]_0$, the bifurcation condition appears to require a fixed rate of consumption of Br^-, which must be provided by input at this rate. We will now show this interpretation is correct, and derive the equation for the lower left side of the SN region, where an SN^+ bifurcation occurs on Fig. 5.

Table II ranks the currents and shows which are essential. $\mathbf{E}_7$ is the flow-through current of BrO_3^-, $\mathbf{E}_8$ is the flow-through current of Ce^{3+}, $\mathbf{E}_{15}$ is a stabilizing current, and $\mathbf{E}_{51}$ is the only essential current that is unstable (see Fig. 10). It closely resembles destabilizing current $\mathbf{E}_{12}$ which produces the Hopf region, but with two key differences. In $\mathbf{E}_{51}$ Br^- is an input, whereas in $\mathbf{E}_{12}$ it is produced by $R_{6.5}$. In $\mathbf{E}_{51}$ Ce^{4+} washes out, whereas in $\mathbf{E}_{12}$ it is consumed by $R_{6.5}$. Because $\mathbf{E}_{51}$ requires an input of Br^- and a high enough flow rate to wash out Ce^{4+}, this current destabilizes at larger values of k_0 and $[Br^-]_0$ than $\mathbf{E}_{12}$.

Why should $\mathbf{E}_{12}$ produce oscillations and $\mathbf{E}_{51}$ produce bistability? Both currents have the same destabilizing positive feedback cycle between Br^- and $HBrO_2$. However, $\mathbf{E}_{12}$ has a large negative feedback cycle that uses Ce^{4+} while $\mathbf{E}_{51}$ does not. How this negative feedback produces oscillations instead of bistability will be explained in Sec. XII.

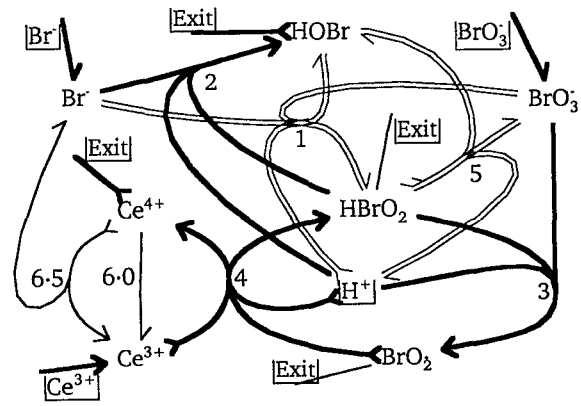

FIG. 10. Extreme current $\mathbf{E}_{51}$ destabilizes the saddle node region. This current differs from $\mathbf{E}_{20}$ in Fig. 9 by using the influx of Br^- rather than R_1 as the source of Br^-. $\mathbf{E}_{51}$ becomes significant at an even higher flow rate and high $[Br^-]_0$.

Deleting nonessential currents yields an approximate network whose steady state manifold (Fig. 11) contains the fold, but none of the other bifurcation points. The $\alpha_d=0$ curve for this approximate network is a straight line with slope -1, which is shown as curve (a) in Fig. 12.

An equation for this line using the essential currents was derived using SNA symbolic algebra software. The resulting equation $j_{15}=j_{51}$ agrees with Table II which shows that the ranking of these currents changes at the bifurcation point. The approximate network is simple enough to solve for the steady states in terms of the (**k**,**C**) parameters. The bifurcation equation $j_{15}=j_{51}$ becomes

$$k_0[Br^-]_0=(6k_1k_3/k_2)[H^+]^2[BrO_3^-]_0^2, \tag{29}$$

which is the straight line in the figure. The rate constants used to plot the line are not the original rate constants but (**k**,**C**) parameters which were recalculated from the (**h**,**j**) parameters after deleting currents.

The straight line approximation gets steadly worse at higher flow rates because none of the essential currents contains the CSTR exit reaction for Br^-. Since the only

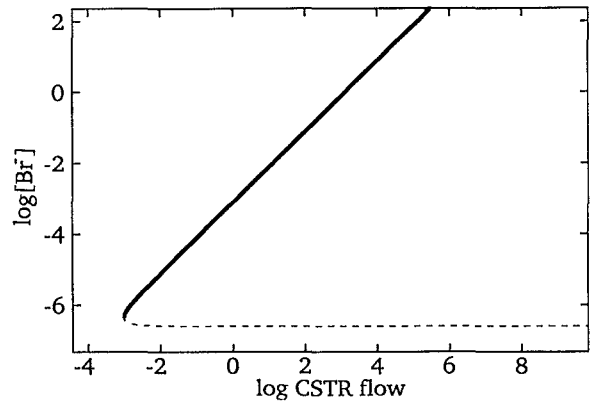

FIG. 11. Deleting extreme currents to simplify a network at a bifurcation point simplifies the steady state manifold. The steady state manifold near the SN^+ bifurcation (c) in Fig. 5 is shown when all but essential currents are deleted.

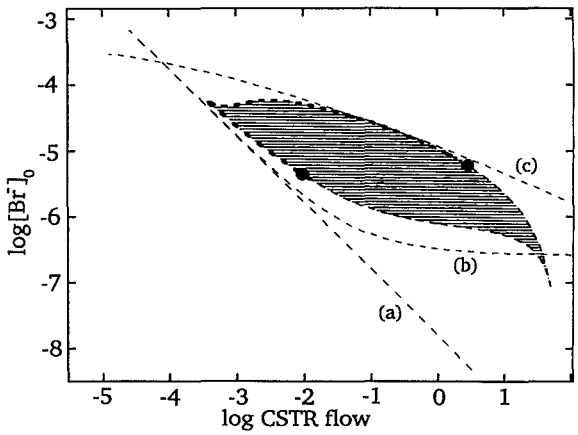

FIG. 12. The multiple steady state region of the phase diagram is shown along with three approximate SN–SN$^+$ bifurcation curves. Curve (a) is the bifurcation curve of only the essential currents [Eq. (29)]. Curve (b) is Eq. (30). Curve (c) is for the network of essential currents at the high flow SN–SN$^+$ bifurcation.

consumption of Br^- in the approximate network is by the network's internal reactions, only a small input concentration $[Br^-]_0$ is needed at high k_0 to supply Br^- at the required rate. However, the calculated phase diagram contains the CSTR exit reaction and most input Br^- washes out at high flow rate. The calculated phase diagram requires a much higher input concentration to provide Br^- at the rate needed for bifurcation and extra Br^- to wash out.

To correct Eq. (29) we include current $\mathbf{E}_6$ which represents entrance and exit of Br^-. The bifurcation condition $j_{15}=j_{51}$ now yields a better approximation which is plotted as curve (b) in Fig. 12

$$k_0=\frac{6k_1k_3[H^+]^2[BrO_3^-]_0^2}{k_2[Br^-]_0-2k_3[BrO_3^-]_0}. \tag{30}$$

The curve becomes horizontal when the denominator vanishes. Multistability only occurs when $[Br^-]_0$ is greater than

$$[Br^-]_0=(2k_3/k_2)[BrO_3^-]_0. \tag{31}$$

This equation can be derived by a very simple argument. Since R_2 is used by both $\mathbf{E}_{15}$ and $\mathbf{E}_{51}$, Eq. (4) gives $v_2=j_{15}+j_{51}$. But R_3 is only used by $\mathbf{E}_{51}$ and Eq. (4) gives $v_3=j_{51}$. Hence when $j_{15}=j_{51}$ it follows that $v_2=2v_3$, which is Eq. (31).

Ringland found that the region of bistability in the experimental system occurs at a much higher level of $[Br^-]_0$ than in his calculations on the SNB model. Eqs. (30) and (31) show that increasing k_3 raises the position of the curves. However, we found that the high-flow Hopf bifurcation was stabilized by a detailed balanced current in R_3, and k_3 had to be reduced to match experiments. These contradictory requirements are the reason why Ringland could not make the network agree with experiments.

The bifurcation condition requires a certain consumption rate of Br^- which must be supplied by the input. Any other process that consumes bromide, such as washing out, requires an even larger $[Br^-]_0$ to compensate.

The SN$^+$ curve will therefore be moved to higher $[Br^-]_0$ if there are reactions which consume Br^- in the experimental system that are left out of the SNB model. Reactions such as $Br^-+HOBr+H^+\rightarrow Br_2+H_2O$ or reactions with organic species could easily consume enough Br^- to explain the experimental location of the SN$^+$ bifurcation curve.

A similar analysis of the high-flow side of the SN region yields the equation $j_{51}=j_3$, which is plotted as curve (c) in Fig. 12. This condition represents stabilization of $\mathbf{E}_{51}$ by detailed balance in R_3, similar to high-flow stabilization of $\mathbf{E}_{12}$ in the Hopf region by R_3.

XI. NEAR THE TAKENS–BOGDANOV POINT

The phase diagram in the (**h**,**j**) parameters near a Takens–Bogdanov (TB) point should resemble Fig. 2(a); however, none of the phase diagrams of the approximate networks examined so far have crossing hypersurfaces $\alpha_d=0$ and $\Delta_{d-1}=0$. That is, no SN or SN$^+$ bifurcations appear for approximate networks used near Hopf bifurcations, and no Hopf bifurcations appear for approximate networks used near SN and SN$^+$ bifurcations.

Since $\mathbf{E}_{12}$ was responsible for the Hopf bifurcations and $\mathbf{E}_{51}$ was responsible for the SN and SN$^+$ bifurcations, an approximate network containing $\mathbf{E}_{12}$ and $\mathbf{E}_{51}$ plus suitable stabilizing currents should have the desired crossing. Table II shows the ranking of the currents at the lower left TB point. The four essential currents in the left SN$^+$ bifurcation are the top four currents at the TB point. Using these guarantees SN and SN$^+$ bifurcations occur in the approximate network. Essential current $\mathbf{E}_{12}$ is next in importance. It should destabilize and produce a Hopf bifurcation region. The important stabilizing currents at the Hopf bifurcations were $\mathbf{E}_4$, $\mathbf{E}_3$, and $\mathbf{E}_{20}$. Of these, only $\mathbf{E}_4$ is large near the TB point. It will be used.

An analysis was made to see if a phase diagram similar to Fig. 2 could be obtained. The analysis yielded 64 systems of inequalities containing a total of 1698 inequalities. The desired cross sections are shown in Fig. 13. This (**h**,**j**) phase diagram contains some unexpected features that are due to the cross-sections being parallel and very close to a bifurcation hypersurface in other dimensions.

XII. HOW UNSTABLE FEEDBACK CYCLES AFFECT THE PHASE DIAGRAM

The phase diagram has two unstable regions, a Hopf region produced by current $\mathbf{E}_{12}$, and an SN region produced by $\mathbf{E}_{51}$. This section shows how a large negative feedback cycle in $\mathbf{E}_{12}$ that is missing from $\mathbf{E}_{51}$ accounts for the different bifurcations of the two unstable currents.

The instability involves three species: Br^-, $HBrO_2$, and BrO_2. A positive feedback 2-cycle between Br^- and $HBrO_2$ using R_2 destabilizes because $HBrO_2$ reproduces itself in an autocatalytic critical current 2-cycle involving BrO_2. This combination of feedback cycles occurs in both destabilizing currents $\mathbf{E}_{12}$ and $\mathbf{E}_{51}$.

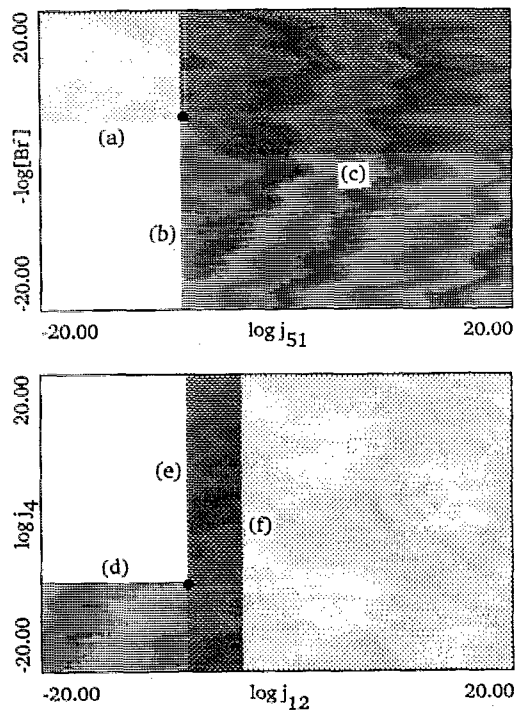

FIG. 13. Two (**h**,**j**) phase diagrams near the low-flow Takens–Bogdanov point. The upper phase diagram is similar to Fig. 1. The types of bifurcations must be inferred from the shading because the software does not outline the regions and draw bifurcation curves. An illusion makes the lower cross section appear to have no Hopf region close to the TB point. The illusion is caused by taking the cross section parallel to the boundary of the Hopf bifurcation region. The marked bifurcation curves are determined by the following conditions for instability: (a) $j_{12}[Ce^{4+}] > j_{15}[Br^-]$, (b) $j_{12}j_{51} > j_{15}^2$, (c) $[BrO_3^-] > [Br^-]$, (d) $j_{51} > j_4$ and (e) $j_{12} > 3j_{51}$. Line (f) is $j_7 j_{51} = j_{15} j_{12}$.

The key difference is the presence of a negative feedback cycle in $\mathbf{E}_{12}$ which is missing from $\mathbf{E}_{51}$. In this cycle an increase in $HBrO_2$ produces an increase in BrO_2 via R_3, which produces an increase in Ce^{4+} via R_4, which produces an increase in Br^- via $R_{6,5}$, which produces a decrease in $HBrO_2$ via R_2.

According to a graph theoretical approach to stability analysis developed by Clarke,[9,10] each term in a characteristic equation coefficient polynomial $\alpha_i(\mathbf{h},\mathbf{j})$ can be interpreted as a product of feedback cycles involving a set of i distinct intermediates. Negative feedback cycles produce positive terms. Positive feedback cycles produce negative terms. Whenever negative terms make $\alpha_i < 0$, the steady state is unstable. Hence, positive feedback cycles make $\alpha_i < 0$ and produce unstable regions.

The destabilizing positive feedback cycles are the same in $\mathbf{E}_{12}$ and $\mathbf{E}_{51}$. Because they involve three species they produce negative terms in α_3, α_4, α_5, α_6, and α_7 (provided α_7 does not vanish from a conservation condition) for both currents.

The negative feedback cycle found only in $\mathbf{E}_{12}$ involves four species, so positive terms are produced in α_i for $i \geqslant 4$. The cycle involves Br^- plus the three species causing instability. Hence it cancels negative terms produced by the destabilizing positive feedback cycles. At the low-flow Hopf bifurcation only α_3 and α_4 have negative terms because negative terms in $\alpha_5,\ldots,\alpha_d$ are cancelled. Similarily, at the high-flow Hopf bifurcation only α_3, α_4, and α_5 have negative terms. Since α_d contains no negative terms, an SN region is impossible. Instability produces a Hopf region.

Because the large negative feedback cycle is missing from $\mathbf{E}_{51}$, destabilizing positive feedback cycles produce negative terms in all coefficients α_i for $i=3,\ldots,d$. It is interesting that when $\mathbf{E}_{51}$ is the only source of instability, α_d is always the first to change sign at the bifurcation point, and only an SN region is produced. Why do the negative terms in some α_i for $i<d$ not produce a sign change first and cause a Hopf bifurcation? The answer must be combinatorics. When i is larger there are more combinations of other intermediates that can combine with the three destabilizing species to produce negative terms. Combinatorics explains why, as a rule, the α_i with the largest i changes sign first.

Section II explained that several Hurwitz determinants often change sign at almost the same **p**, that the Hurwitz determinants could be approximated by the product of diagonal terms, and that the first row of the Routh array can be approximated as $\mathsf{R}=(1,\alpha_1,\alpha_2,\ldots,\alpha_{d-1},\alpha_d)$. The validity of these approximations, called the *α-approximation*, will now be examined.

The α-approximation affects only the Hopf region. When positive feedback cycles make α_3, α_4, or α_5 negative the steady state must already be unstable. The exact bifurcation point must occur when $\Delta_{d-1}=0$, while α_3, α_4, and α_5 are still positive. The α-approximation is valid when this difference is small enough to be considered negligible.

To test the α-approximation, the Hopf bifurcation points on Fig. 5 were calculated using $\Delta_d(\mathbf{k},\mathbf{C})=0$ and $(\mathbf{k},\mathbf{C})$ was placed at a bifurcation point. Then the corresponding $(\mathbf{h},\mathbf{j})$ was located on a plot showing the regions $\alpha_3<0$, $\alpha_4<0$ and $\alpha_5<0$. These regions coincided closely (at the scale of the phase diagram), and $(\mathbf{h},\mathbf{j})$ was found on their common boundary. Hence, the sign changes in $\Delta_d,\alpha_3,\alpha_4,\alpha_5$ occur almost simultaneously.

The α-approximation is justified using a method for determining the important terms, called Newton's polygon[28] for two-variable polynomials, and exponent polytopes[29] for n-variable polynomials. The α approximation works because the exponents of diagonal terms in the Hurwitz determinant Eq. (8) lie on a sphere of larger radius than other terms.[10] Terms from the polynomials on this sphere are dominant. Ignoring nondominant terms eliminates all of Δ_i but the diagonal terms. Consequently, crossing a small step into the unstable region at the low and high-flow Hopf bifurcations causes the sign pattern in first row of the Routh array to change to $(+,+,-,-,+,+,+)$ and $(+,+,-,-,-,+,+)$, respectively. At the SN and SN^+ bifurcations the sign pattern becomes $(+,+,-,-,-,-,-)$. Reasonably accurate phase diagrams can be calculated from $\alpha_i=0$ for various i.

Overlapping Hopf and SN regions should occur in many networks with similar features. To produce an SN region, the network must have i species that form positive feedback cycles, and no larger negative feedback cycles

involving all i species. To produce the Hopf region the network needs a larger negative feedback cycle that can prevent the negative terms in α_i from appearing in α_d. When the negative cycle appears in some but not all unstable extreme currents, overlapping Hopf and SN regions and TB points should appear. These often make the phase diagram cross-shaped.

XIII. DISCUSSION

A general method for deriving the main features of dynamical phase diagrams has been given and illustrated using the SNB network. We found that the main features of the SNB phase diagram in Fig. 6 can be described by a small number of equations in the (**h**,**j**) parameters. The visible part of the Hopf region for low $[Br^-]_0$ is bounded by

$$j_{12} \geqslant 3j_1 \quad \text{(low-flow)},$$

$$j_{12} \geqslant 3j_{20} \quad \text{(high-flow)},$$

$$j_{12} \geqslant j_3 \quad \text{(high-flow)},$$

and the two visible sides of SN region are given by

$$j_{51} \geqslant j_{15} \quad \text{(low-flow)},$$

$$j_{51} \geqslant j_3 \quad \text{(high-flow)}.$$

The 2-dimensional cross section in Fig. 6 does not convey the great complexity of the actual unstable region in the high-dimensional parameter space. Some idea of the true complexity can be appreciated from the fact that hundreds of inequalities are needed to describe it.

While these equations are based on essential currents, the accuracy of the phase diagram curve can be improved by including nonessential currents. For example, curve (b) in Fig. 12 is a more accurate plot of $j_{51}=j_{15}$ than curve (a) because the exit pseudoreaction for Br^- is included. Any nonessential reactions which affect $[Br^-]$ affect the curve's location. Reactions that consume Br^- move the curve to larger $[Br^-]_0$ in better agreement with the calculations.

Ringland found that the SNB network could not be matched to experiment because conflicting changes in rate constants were needed. We have shown that adding the Br^- consuming reactions in the real system should help.

Our method should work for most oscillating mechanisms. Starting with the minimum set of essential currents (reactions) that can produce a bifurcation, the method obtains equations in the (**h**,**j**) parameters using SNA software. At present this software can treat networks with approximately 19 intermediates and 1 current, 17 intermediates and 2 currents,..., . A Hopf bifurcation analysis using three currents is practical for mechanisms with as many as 13 intermediates.

Converting the (**h**,**j**) equations to (**k**,**C**) variables can involve some difficult algebra. We saw that appending a known bifurcation equation greatly simplifies the algebraic calculations. In the region of a TB point, SNA can provide a second bifurcation equation, which should make the algebra even simpler.

The method illustrated here can been used to match experimental data for far more complicated networks than the SNB example, whose simplicity makes the method clear.

[1] J. Boissonade and P. de Kepper, J. Phys. Chem. **84**, 501 (1980).
[2] J. Guckenheimer, Physica D **20**, 1 (1986).
[3] F. Dumortier, R. Roussaire, and J. Sotomayor, Ergod. Th. Dynam. Sys. **7**, 375 (1987).
[4] H. Annabi, M. L. Annabi, and F. Dumortier, in *Geometry and Analysis in Nonlinear Dynamics*, edited by H. W. Broer and F. Takens (Longman Scientific and Technical, Harlow, 1991), p. 1.
[5] R. J. Olsen and I. R. Epstein, J. Chem. Phys. **98**, 2805 (1993).
[6] J. Ringland, J. Chem. Phys. **95**, 555 (1991).
[7] R. J. Field and R. M. Noyes, J. Chem. Phys. **60**, 1877 (1974).
[8] K. Showalter, R. Noyes, and K. Bar-Eli, J. Chem. Phys. **69**, 2514 (1978).
[9] B. L. Clarke, J. Chem. Phys. **60**, 1481 (1974).
[10] B. L. Clarke, Adv. Chem. Phys. **43**, 1 (1980).
[11] B. L. Clarke, J. Chem. Phys. **75**, 970 (1981).
[12] B. L. Clarke, in *Chemical Applications of Topology and Graph Theory*, edited by R. B. King (Elsevier, Amsterdam, 1983), p. 322.
[13] B. L. Clarke, Cell Biophys. **12**, 237 (1988).
[14] F. Hynne, P. G. Sørensen, and T. Møller, J. Chem. Phys. **98**, 211 (1993).
[15] F. Hynne, P. G. Sørensen, and T. Møller, J. Chem. Phys. **98**, 219 (1993).
[16] B. L. Clarke, J. Chem. Phys. **97**, 2459 (1992).
[17] B. Porter, *Stability Criteria for Linear Dynamical Systems* (Academic, London, 1968).
[18] L. Orlando, Math. Ann. **71**, 233 (1911).
[19] J. Hale and H. Koçak, *Dynamics and Bifurcations* (Springer-Verlag, New York, 1991).
[20] B. D. Aguda and B. L. Clarke, J. Chem. Phys. **89**, 7428 (1988).
[21] R. J. Field, E. Koros, and R. Noyes, J. Am. Chem. Soc. **94**, 8649 (1972).
[22] M. Kubicek, ACM Trans. Math. Software **2**, 98 (1976).
[23] Wegscheider, Z. Physik. Chem. (Leipzig) **39**, 257 (1901).
[24] Strictly speaking, any steady state **v** is a current. However, we often use the term *current* for brevity when we mean extreme current.
[25] B. L. Clarke, J. Chem. Phys. **97**, 4066 (1992).
[26] The calculation time is for 16-bit SNA software running in OS/2 1.21 using a Compaq 386/20 personal computer.
[27] M. Eiswirth, A. Freund, and J. Ross, J. Phys. Chem. **95**, 1294 (1991).
[28] I. Newton, in *The Mathematical Papers of Isaac Newton 1670–1673*, edited by D. T. Whiteside (Cambridge University, Cambridge, 1969), p. 50.
[29] B. L. Clarke, SIAM J. Appl. Math. **35**, 755 (1978).